Warm dust resolved in the cold disk around T Chamaeleontis with VLTI/AMBER

J. Olofsson, M. Benisty, J. -C. Augereau, C. Pinte, F. Ménard, E. Tatulli, J. -P. Berger, F. Malbet, B. Merín, E. F. van Dishoeck, et al.

▶ **To cite this version:**

J. Olofsson, M. Benisty, J. -C. Augereau, C. Pinte, F. Ménard, et al.. Warm dust resolved in the cold disk around T Chamaeleontis with VLTI/AMBER. Astronomy and Astrophysics - A&A, 2011, 528, 10.1051/0004-6361/201016074 . insu-03625200

HAL Id: insu-03625200

https://insu.hal.science/insu-03625200

Submitted on 30 Mar 2022

HAL is a multi-disciplinary open access archive for the deposit and dissemination of scientific research documents, whether they are published or not. The documents may come from teaching and research institutions in France or abroad, or from public or private research centers.

L'archive ouverte pluridisciplinaire **HAL**, est destinée au dépôt et à la diffusion de documents scientifiques de niveau recherche, publiés ou non, émanant des établissements d'enseignement et de recherche français ou étrangers, des laboratoires publics ou privés.

Distributed under a Creative Commons Attribution| 4.0 International License

A&A 528, L6 (2011)
DOI: 10.1051/0004-6361/201016074
© ESO 2011

Astronomy & Astrophysics

Letter to the Editor

Warm dust resolved in the cold disk around T Chamaeleontis with VLTI/AMBER⋆

J. Olofsson[1], M. Benisty[1], J.-C. Augereau[2], C. Pinte[2], F. Ménard[2], E. Tatulli[2], J.-P. Berger[3], F. Malbet[2], B. Merín[4], E. F. van Dishoeck[5,6], S. Lacour[7], K. M. Pontoppidan[8], J.-L. Monin[2], J. M. Brown[6], and G. A. Blake[8]

[1] Max Planck Institut für Astronomie, Königstuhl 17, 69117 Heidelberg, Germany
e-mail: olofsson@mpia.de
[2] UJF-Grenoble 1/CNRS-INSU, Institut de Planétologie et d'Astrophysique de Grenoble (IPAG) UMR 5274, 38041 Grenoble, France
[3] ESO, Alonso de Crdova 3107, Vitacura, Casilla 19001, Santiago de Chile, Chile
[4] Herschel Science Centre, SRE-SDH, ESA PO Box 78, 28691 Villanueva de la Cañada, Madrid, Spain
[5] Leiden Observatory, Leiden University, PO Box 9513, 2300 RA Leiden, The Netherlands
[6] Max Planck Institut für Extraterrestrische Physik, Giessenbachstrasse 1, 85748 Garching, Germany
[7] Observatoire de Paris, LESIA/CNRS (UMR 8109), 5 place Jules Janssen, 92195 Meudon, France
[8] California Institute of Technology, Division of Geological and Planetary Sciences, MS 150-21, Pasadena, CA 91125, USA

Received 4 November 2010 / Accepted 4 January 2011

ABSTRACT

Context. The transition between massive Class II circumstellar disks and Class III debris disks, with dust residuals, has not yet been clearly understood. Disks are expected to dissipate with time, and dust clearing in the inner regions can be the consequence of several mechanisms. Planetary formation is one of them that will possibly open a gap inside the disk.
Aims. According to recent models based on photometric observations, T Cha is expected to present a large gap within its disk, meaning that an inner dusty disk is supposed to have survived close to the star. We investigate this scenario with new near-infrared interferometric observations.
Methods. We observed T Cha in the *H* and *K* bands using the AMBER instrument at VLTI and used the MCFOST radiative transfer code to model the SED of T Cha and the interferometric observations simultaneously and to test the scenario of an inner dusty structure. We also used a toy model of a binary to check that a companion close to the star can reproduce our observations.
Results. The scenario of a close (few mas) companion cannot satisfactorily reproduce the visibilities and SED, while a disk model with a large gap and an inner ring producing the bulk of the emission (in *H* and *K*-bands) close to 0.1 AU is able to account for all the observations.
Conclusions. With this study, the presence of an optically thick inner dusty disk close to the star and dominating the *H* and *K*-bands emission is confirmed. According to our model, the large gap extends up to ∼7.5 AU. This points toward a companion (located at several AU) gap-opening scenario to explain the morphology of T Cha.

Key words. stars: pre-main sequence – stars: evolution – protoplanetary disks – circumstellar matter – infrared: stars – techniques: interferometric

1. Introduction

Using the IRAS space observatory, Strom et al. (1989) have reported that several pre-main-sequence stars show a lack of emission in the mid-infrared (IR) compared to their far-IR flux, owing to a lack of warm dust indicative of the early stages of planetary formation. Several Herbig Ae/Be stars also show very similar properties in their spectral energy distribution (SED hereafter), such as HD100546 (Bouwman et al. 2003) observed with *ISO*. Thanks to the great sensitivity of the *Spitzer* Space Telescope, fainter T Tauri stars were found to present such behavior (e.g., Brown et al. 2007). These so-called "cold disks" are suspected to represent one of the transitional stages between the dust and gas-rich Class II objects and the Class III stars with only dust and gas residuals. The lack of emission in the mid-IR domain has been interpreted as a tracer for dust clearing in the first AU of the circumstellar disks. Several mechanisms can be responsible for dust clearing, such as a binary companion (Jensen & Mathieu 1997) which is the case for CoKu Tau 4 (Ireland & Kraus 2008), or photo-evaporation processes (Alexander et al. 2006). These mechanisms will clear the disk as probed by submillimeter and millimeter observations (e.g., Andrews et al. 2009; Hughes et al. 2009; Brown et al. 2009). Another dust-clearing process is the formation of a planet inside the disk. Because the planet is accreting surrounding material, a gap may open within the disk, resulting in an inner and an outer disks (e.g., Varnière et al. 2006).

In this Letter, we present the first near-IR interferometric observations of a T Tauri star by the AMBER instrument, installed at the Very Large Telescope Interferometer (VLTI, Schöller 2007). T Cha (spectral type G8) is one of the four cold disks studied by Brown et al. (2007). To model the SED of T Cha, and especially the *Spitzer*/IRS spectrum, they needed two separated

⋆ Based on AMBER observations collected at the VLTI (European Southern Observatory, Paranal, Chile) with open time programs 083.C-0295(A,B).

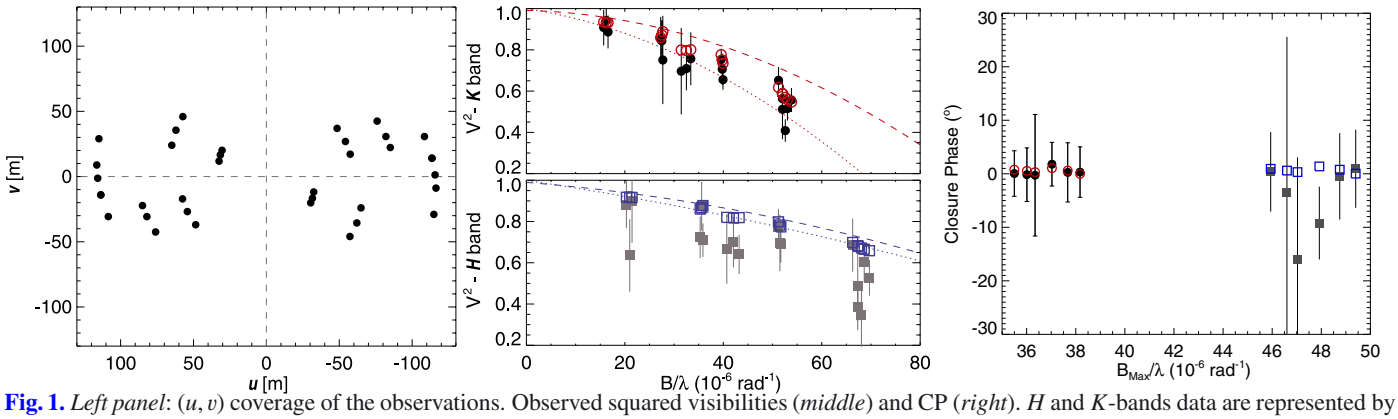

Fig. 1. *Left panel*: (u, v) coverage of the observations. Observed squared visibilities (*middle*) and CP (*right*). H and K-bands data are represented by squares and circles symbols, respectively. Overplotted are the predictions from our best disk model (empty symbols). Dashed and dotted lines in the middle panels are a 2nd-order polynomial fit the modeled visibilities for the extreme values on $R_{\rm in,\,inner\,disk}$ within the uncertainties (see Sect. 3).

regions in the disk: an inner low-mass radially confined belt (from 0.08 to 0.2 AU) and a massive outer disk (15–300 AU). The first component accounts for the excess emission at wavelengths shorter than 10 μm, while the second accounts for the emission at longer wavelengths. The large gap allows the lack of emission around 10 μm to be reproduced. As the presence of a gap may suggest there are substellar companions, T Cha would therefore become a prime target when searching for planets. Unfortunately, SED fitting is highly degenerated, therefore we acquired spatially resolved observations at high angular resolution with the near-IR instrument, AMBER, at the VLTI to lift some of the degeneracies in the SED fitting process, to confirm the presence of the inner disk, and study its structure.

We first describe, in Sect. 2, the AMBER observations and their reduction, as well as first simple models used to interpret these data. In Sect. 3 we present radiative transfer models that we use to reproduce the SED and interferometric observables simultaneously, and we finally conclude with the results in Sect. 4.

2. Results and first analysis

2.1. VLTI/AMBER observations

T Cha was observed at the VLTI, using the AMBER instrument that allows the simultaneous combination of three beams in the near-IR with spatial filtering (Petrov et al. 2007). The instrument delivers spectrally dispersed interferometric visibilities, closure phases (CP hereafter), and differential phases at spectral resolutions up to 12 000. In the following, we present K- and H-bands (around 2.2 and 1.65 μm, respectively) observations taken in the low spectral resolution mode (LR; $R \sim 35$) with the 8.2 m Unit Telescopes (UTs), coupled with the use of adaptive optics. T Cha was observed with 5 different baselines of two VLTI configurations (UT1-2-4 and UT1-3-4), during June 11 and 12, 2009. The longest baseline length is ~130 m corresponding to a maximum angular resolution of 1.3 milli-arcseconds (mas). The integration time per frame was 50 ms. In addition to T Cha, a calibrator (HD 107145, F5V) was observed to correct for instrumental effects. Observations were performed without fringe-tracking.

Data was reduced following the standard procedures described in Tatulli et al. (2007) and Chelli et al. (2009), using the `amdlib` package, release 2.99, and the `yorick` interface provided by the Jean-Marie Mariotti Center (`http://www.jmmc.fr`). Raw spectral visibilities and CP were extracted for all the frames of each observing file. A selection of 80% of the highest quality frames was made to minimize the effect of instrumental jitter and non-optimal light injection into the instrument. The AMBER+VLTI instrumental transfer function was calibrated using measurements of HD 107145, after correcting for its diameter (0.3 ± 0.1 mas, which was obtained using the getCal software, `http://nexsciweb.ipac.caltech.edu/gcWeb/gcWeb.jsp`). The H-band measurements have a lower signal-to-noise ratio since they have been obtained close to the instrument-limiting magnitude. With about 20 spectral channels through the H and K bands, the total data set (after processing) is made of 585 and 195 spectrally dispersed visibilities and CP, respectively (averaged for each baseline and baseline triplet to provide 36 and 12 broad-band visibilities and CP, respectively).

Figure 1 presents the final reduced data for T Cha: the (u, v) coverage (left panel), the squared visibilities in H and K broad bands as a function of the spatial frequencies (gray and black, respectively, middle panel), and the CP (right panel). The squared visibilities show that the circumstellar emission around T Cha is marginally resolved: the squared visibilities decrease with increasing spatial frequency, but remain at a high level ($V^2 \geq 0.3$). We do not observe strong discrepancies between H and K bands visibilities, suggesting that the same structure is responsible for most of the emission in H and K bands. Finally, the CP are close to zero, indicative of a centro-symmetric structure at the given spatial resolution of the observations. We first investigate the possibility of a companion around T Cha, and then examine whether an inner dusty disk as proposed by Brown et al. (2007) can reproduce the data.

2.2. Geometric models

To see whether our interferometric datapoints are compatible with a companion around T Cha, we used a toy model that aims to describe a binary system where both stars are individually unresolved (e.g., Lawson 1999). To find a model that best reproduces both AMBER visibilities and CP, we performed a χ^2 minimization exploration through a 3-dimensional grid: flux ratio between the two components (F_2/F_1), separation (ρ), and position angle (PA). The reduced $\chi^2_{\rm r}$ values are then transformed into normalized probabilities to perform a statistical (Bayesian) analysis. The top three panels of Fig. A.1 display the reduced $\chi^2_{\rm r}$ maps for the three pairs of free parameters. We derived uncertainties from the probability distributions. The binary parameters for the best model ($\chi^2_{\rm r} = 0.29$) are the following: flux ratio of $F_2/F_1 = 0.95^{+0.05}_{-0.85}$, separation of $\rho = 1.15^{+0.57}_{-0.49}$ mas, and position

angle on the sky of PA = $68^{\circ}{}^{+25}_{-68}$ east of north. The uncertainty on the flux ratio is rather large, because the squared visibilities (36 values) can also be reproduced for a small-flux ratio. However, in that case, CP (12 values) are not close to zero and CP are only matched for higher flux ratio, close to unity. The large uncertainties on F_2/F_1 therefore reflect the larger amount of visibility with respect to the number of CP. That the flux ratio is about $F_2/F_1 \sim 1$ implies that the emission profile of the companion, if any, would be similar to the one of the primary and not colder, as expected in order to match the near-IR excess probed from SED modeling (Brown et al. 2007). Besides this consideration, Schisano et al. (2009) conclude from radial velocity measurements, that even a low-mass object (0.05 $M_{\odot}$) at a distance of 0.1 AU would have been detected. Additionally, NaCo narrow-band imaging observations of T Cha at 2.12 and 1.75 μm rule out any stellar companion with a mass higher than 0.15 $M_{\odot}$ between ~2 and 10 AU (Vicente et al., submitted). A close companion in the first tenths of AU around T Cha is therefore not a satisfying solution.

We now consider the case of a uniform ring aimed at representing the inner disk edge (e.g., Eisner et al. 2004). The three input variables of this model are the position angle of the disk (PA, 0°, meaning the major semi-axis is oriented north-south), the inclination on the line of sight (i, 0° is face-on), and the inner diameter (θ). We fixed the star-to-ring flux ratio to account for H and K band excess derived using a Nextgen synthetic spectrum of the star (see Sect. 3.2). The width W of the uniform ring is given by $W/(\theta/2) = 0.18$. We performed a grid exploration for these three parameters, with a $\chi^2_{\rm r}$ minimization. The bottom three panels of Fig. A.1 show the reduced $\chi^2_{\rm r}$ maps for the three pairs of free parameters. Only the diameter is determined well with this approach, while the position angle and inclination cannot be strongly constrained, because of the almost unidirectional alignment of the (u, v) points. The final best fit ($\chi^2_{\rm r} = 0.76$) returns PA = $67^{\circ}{}^{+91}_{-56}$, $i = 42^{\circ}{}^{+32}_{-40}$, and $\theta = 1.82^{+0.52}_{-0.38}$ mas. Therefore, a dust ring model at a tenth of AU or so from the star is consistent with the AMBER visibilities and with the photometric excesses in the H- and K-bands. Nonetheless, the above model is an oversimplified description of a disk and ignores the disk's asymmetry, as well as the SED at other wavelengths. We develop a refined model in the next section.

3. Radiative transfer modeling

Hipparcos has estimated a 66^{+19}_{-12} pc distance for T Cha, but, as explained in Schisano et al. (2009), proper motions measurements by Frink et al. (1998) and Terranegra et al. (1999) suggest that this distance is underestimated. T Cha may in fact belong to a star association cluster located at 100 pc, which is the distance that we adopt in this study. The disk inclination is also uncertain. An inclination of 75° is commonly used in the literature. This value comes from $v \sin i$ measurements (54 km s^{-1}, Alcalá et al. 1993) indicative of a highly inclined object. Schisano et al. (2009) measured $v \sin i$ of 37 ± 2 km s^{-1}, which could suggest a slightly smaller inclination. However, T Cha displays CO in absorption in the 4.7 μm fundamental band (Brown et al., in prep.), which requires a high inclination (~60–70°). In the following, the inclination is therefore considered as a free parameter and is further discussed in Sect. 3.2.

3.1. Model setup

To model the disk emission and to reproduce simultaneously, the squared visibilities and CP in H & K bands, as well as the SED, we used the MCFOST radiative transfer code (Pinte et al. 2006). MCFOST calculates synthetic observables, such as SEDs and monochromatic raytraced images. The computation is done by propagating packets of photons inside the disk. Light scattering, absorption, and re-emission processes are included. The geometry of the disk is defined by several parameters: the inner and outer radii ($R_{\rm in}$ and $R_{\rm out}$, respectively), the index α for the surface density ($\Sigma(r) = \Sigma(r/r_0)^{\alpha}$), and a disk scale height $H(r)$ assuming a vertical Gaussian distribution ($\exp[-z^2/2H(r)^2]$), germane to a disk at the hydrostatic equilibrium. The disk's flaring is described by a powerlaw determining the scale height as a function of the radius ($H(r) = H_0(r/r_0)^{\beta}$). The dust content is described by a differential powerlaw for the grain size distribution ($\mathrm{d}n(a) \propto a^{-p}\mathrm{d}a$), between the minimum ($a_{\rm min}$) and maximal ($a_{\rm max}$) grain sizes. The radiative transfer code can handle spatially separated disk zones.

3.2. Results and discussion

To reproduce the stellar photosphere, we adopt a NextGen stellar atmosphere model (Allard et al. 1997). All the stellar parameters, except the inclination i, were taken from Brown et al. (2007). The two parameters $T_{\rm eff}$ and R_* were then varied only to remain unchanged once the $UBVRI$ bands were reproduced well enough. In the end, the star is defined with the following parameters: $T_{\rm eff} = 5400$ K, $\log(g) = 3.5$, $R_* = 1.3\,R_{\odot}$, $M_* = 1.5\,M_{\odot}$, and $A_{\rm v} = 1.5$.

The disk is known to have a depleted zone (gap) according to SED modeling (Brown et al. 2007). Therefore, two separate zones were defined for the circumstellar material: an inner and an outer dusty structure. Given the high angular resolution of our observations, the outer disk is overresolved, so changing its characteristics will only affect the SED. For the inner disk we use a mixture of astro silicates (Draine & Lee 1984) and amorphous carbon (Zubko et al. 1996) with a mass ratio of 4:1 between silicate and carbon. We choose to use this composition, because these grains will produce a very weak emission feature at 10 μm, which has not been detected in the IRS spectrum (Brown et al. 2007). From previous tests with different compositions (e.g., less carbon), such features, even a small one, will fill the dip in the 7–15 μm range and will not produce a good fit to the SED. We try using larger grains (≥10 μm) to avoid any emission features, without any satisfying results on both visibilities and SED. In our model,the dust mass of the inner disk is $10^{-9}\,M_{\odot}$, and falls in the optically thick regime. The near-IR excess cannot be reproduced by an optically thin inner disk. However, as the AMBER observations only trace the $\tau = 1$ surface, further constraints on the inner disk mass cannot be established. For the outer disk, we use grain opacities of astro silicates, and the total dust mass of the outer disk, for grain sizes up to 3 mm, of $[1.75 \pm 0.25] \times 10^{-4}\,M_{\odot}$ is constrained well by the millimeter observations. We choose to use an inclination of 60°, while 75° is often used in the literature. With an inclination higher than 60°, the outer disk hides the inner disk, which would account neither for the NIR excess nor for the interferometric measurements. Even if the PA does not affect the SED, it affects the modeled visibilities and CP. It is therefore important to estimate a reasonable value. We use the uniform ring model described in Sect. 2.2, with a fixed inclination of 60°. The best PA is in that case $78^{\circ}{}^{+87}_{-50}$, and even if not well-constrained, we use this value when computing visibilities from ray-traced images.

The best model ($\chi^2_{\rm r} = 0.58$) is found using a grid of models on the following parameters: $R_{\rm in}$, $R_{\rm out}$, $M_{\rm dust}$, and H/R for the inner disk, starting from the model described in

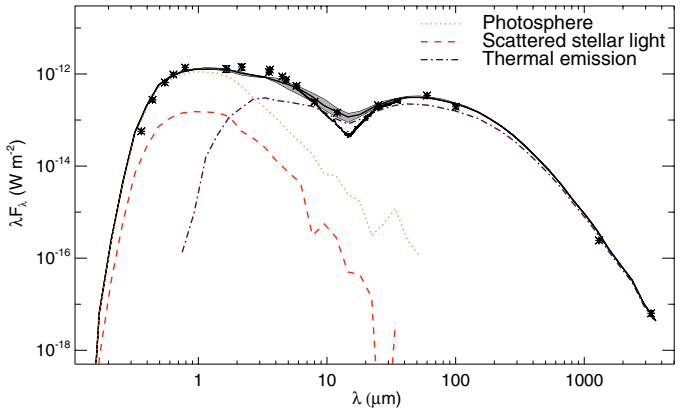

Fig. 2. Observed and modeled SED of T Cha. Photometric measurements were gathered from the literature (Brown et al. 2007; Lommen et al. 2010; Alcalá et al. 1993, and reference therein). The gray area represents the modeled SED for the extreme values on $R_{\rm in,\,inner\,disk}$, within the uncertainties (see Sect. 3).

Table 1. Parameters of the disk model.

Parameter	Inner disk	Outer disk
Size distribution index p	–3.5	–3.5
$a_{\rm min} - a_{\rm max}$ [μm]	0.1–10	0.01–3000
$M_{\rm dust,disk}$ [$M_\odot$]	1×10^{-9}	$1.75 \pm 0.25 \times 10^{-4}$
$R_{\rm in}$ [AU]	0.13 ± 0.03	7.5 ± 0.5
$R_{\rm out}$ [AU]	0.17 ± 0.03	300
Flaring index (β)	1.11	1.11
H/R (at 1 AU)	0.106	0.15
Surface density index (α)	–1	–1

Brown et al. (2007). Similar models are then computed for different grain compositions and sizes. Once the visibilities and near-IR excess are reproduced well, we fine-tune the outer disk's setup in order to match the far-IR and mm observations. All the parameters of the disk model are compiled in Table 1. The visibilities and CP for the best model, calculated for the same (u, v) points (left panel of Fig. 1) as the observations, are presented on the middle and right panels of Fig. 1, respectively and the final SED is displayed in Fig. 2. Modeled visibilities are slightly overestimated compared to observations, especially in the H-band, but lie within the uncertainties. Our model reproduces well the overall decrease of the visibilities. Middle panels of Fig. 1 also show the influence of the location of the inner ring models for the two extreme cases of $R_{\rm in,\,inner\,disk} = 0.1$ and 0.16 AU, respectively, with $R_{\rm out,\,inner\,disk} = R_{\rm in,\,inner\,disk} + 0.04$ AU. The CP and SED (except for the abrupt dip around 10 μm) are also reproduced well by our two separate zones radiative transfer model. The influence of the variation of $R_{\rm in,\,inner\,disk}$ in the range 0.13 ± 0.03 AU is also displayed in Fig. 2. This shows that, even with a large uncertainty on the PA and a highly inclined disk, combining both visibilities and SED provides strong constraints on the $R_{\rm in,\,inner\,disk}$ parameter.

By combining the AMBER data and the SED, we constrain the inner dust ring to be even narrower (between 0.13 and 0.17 AU) than what was inferred by Brown et al. (2007, between 0.08 and 0.2 AU). One should note that our solution may not be unique, since material can possibly be hidden at larger distances (few AU), shadowed by the inner disk, but neither interferometric nor SED measurements can reveal such an extension. Nevertheless, the location of the inner disk edge is interestingly found to be almost similar when using MCFOST that includes scattering and a geometric ring model that represents only for the thermal emission ($R_{\rm in} = \theta/2 \sim 0.9$ mas $= 0.09$ AU at 100 pc). This conclusion, in apparent contradiction to Pinte et al. (2008), results from the extreme compactness of the inner disk (width ~ 0.04 AU) that leads to a total emission for which we cannot disentangle the respective contributions of thermal and scattered light emissions. With the inner edge of the inner disk set at 0.13 AU, the dust reaches a maximum temperature of 1337 K, in agreement with carbon and silicate sublimation temperatures. Even if the outer disk is not resolved with our observations, changing the inner disk's setup (position, scale height, and flaring) has a strong impact on the outer structure, because of the shadow cast by the inner disk. We therefore had to shift the inner edge of the outer disk from 15 AU (Brown et al. 2007) down to 7.5 AU, in order to reproduce the SED. Finally, we do not claim to have a precise determination of either i or PA with our observations, considering the poor (u, v) coverage.

4. Conclusion

In Sects. 2 and 3 we presented and modeled the interferometric observations of T Cha obtained with the AMBER instrument. Two models were investigated, and using both near-IR visibilities and SED, we conclude that the scenario of a close companion, in the first tenths of AU, cannot satisfactorily reproduce the observations, while we present a successful radiative transfer disk model that agrees with both interferometric data and SED. With the near-IR visibilities, we spatially resolve and witness the presence of warm dust and we constrain its location ($R_{\rm in,\,inner\,disk}$). The thinness of the ring is derived from combining the interferometric data and the SED, while the gap is deduced solely from the SED. A continuous disk model, without any gap and with an inner rim located at 0.13 AU would also reproduce the near-IR visibilities, CP, and near-IR fluxes ($\chi^2_{\rm r} = 0.54$), but not the overall SED.

Models of gap opening by a Jupiter-mass planet located at 5 AU (e.g., Varnière et al. 2006) predict a gap between ~2 and 8 AU, suggesting either a multiple planet system, a more massive perturber, or an extended self-shadowed disk up to ~2 AU. Interestingly, Huélamo et al. (2011) detected a $<100\,M_{\rm Jup}$ companion located at 6.7 AU from T Cha using sparse aperture masking observations. Future numerical simulations will have to (i) determine if the inner disk can be a consequence of and survive the disk clearing by possible companion(s) and (ii) investigate what the contribution of inward mass transfer is throughout the gap to eventually refill the inner disk. If ignoring erosion mechanisms other than accretion and assuming that no self-shadowed disk is present, the survival of the disk over a few Myr can be ensured if the accretion rate lies below $10^{-13}\,M_\odot\,{\rm yr}^{-1}$ (assuming a gas-to-dust ratio of 100), a value consistent with the upper limit measured by Schisano et al. (2009) to be of about $4 \times 10^{-9}\,M_\odot\,{\rm yr}^{-1}$. Alternatively, we may be witnessing the aftermath of a collision between two planetesimals or planet embryos, resulting in a transient 2.7 $M_{\rm Lunar}$ dust belt around T Cha.

Acknowledgements. The authors thank the anonymous referee for the constructive and useful comments provided. They also thank the Max Planck Society, the Programme National de Physique Stellaire (PNPS) and ANR (contract ANR-07-BLAN-0221) for supporting part of this research. C. Pinte acknowledges funding from the European Commission's 7th Framework Program (contracts PIEF-GA-2008-220891 and PERG06-GA-2009-256513). CNRS is acknowledged for having supported this work with allocation of 0.3 night in guaranteed time observations.

Appendix A: Geometric models

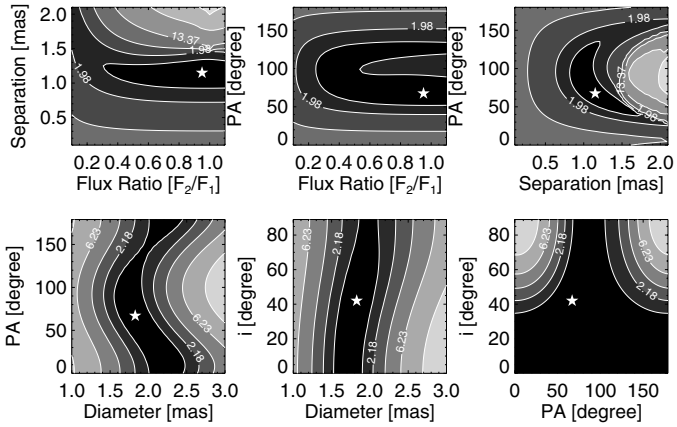

Fig. A.1. *Top panels*: reduced χ^2_r maps for the binary model. *Bottom panels*: reduced χ^2_r maps for the uniform ring model. The star symbol corresponds to values found for the best fit with the lowest reduced χ^2_r.

References

Alcalá, J. M., Covino, E., Franchini, M., et al. 1993, A&A, 272, 225
Alexander, R. D., Clarke, C. J., & Pringle, J. E. 2006, MNRAS, 369, 216
Allard, F., Hauschildt, P. H., Alexander, D. R., & Starrfield, S. 1997, ARA&A, 35, 137
Andrews, S. M., Wilner, D. J., Hughes, A. M., Qi, C., & Dullemond, C. P. 2009, ApJ, 700, 1502
Bouwman, J., de Koter, A., Dominik, C., & Waters, L. B. F. M. 2003, A&A, 401, 577
Brown, J. M., Blake, G. A., Dullemond, C. P., et al. 2007, ApJ, 664, L107
Brown, J. M., Blake, G. A., Qi, C., et al. 2009, ApJ, 704, 496
Chelli, A., Utrera, O. H., & Duvert, G. 2009, A&A, 502, 705
Draine, B. T., & Lee, H. M. 1984, ApJ, 285, 89
Eisner, J. A., Lane, B. F., Hillenbrand, L. A., Akeson, R. L., & Sargent, A. I. 2004, ApJ, 613, 1049
Frink, S., Roeser, S., Alcala, J. M., Covino, E., & Brandner, W. 1998, A&A, 338, 442
Huélamo, N., Lacour, S., Tuthill, P., et al. 2011, A&A, 528, L7
Hughes, A. M., Andrews, S. M., Espaillat, C., et al. 2009, ApJ, 698, 131
Ireland, M. J., & Kraus, A. L. 2008, ApJ, 678, L59
Jensen, E. L. N., & Mathieu, R. D. 1997, AJ, 114, 301
Lawson, P. 1999, Principles of Long-Baseline Stellar Interferometry, ed. P. Lawson
Lommen, D. J. P., van Dishoeck, E. F., Wright, C. M., et al. 2010, A&A, 515, A77+
Petrov, R. G., Malbet, F., Weigelt, G., et al 2007, A&A, 464, 1
Pinte, C., Ménard, F., Berger, J. P., Benisty, M., & Malbet, F. 2008, ApJ, 673, L63
Pinte, C., Ménard, F., Duchêne, G., & Bastien, P. 2006, A&A, 459, 797
Schisano, E., Covino, E., Alcalá, J. M., et al. 2009, A&A, 501, 1013
Schöller, M. 2007, New Astron. Rev., 51, 628
Strom, K. M., Strom, S. E., Edwards, S., Cabrit, S., & Skrutskie, M. F. 1989, AJ, 97, 1451
Tatulli, E., Millour, F., Chelli, A., et al. 2007, A&A, 464, 29
Terranegra, L., Morale, F., Spagna, A., Massone, G., & Lattanzi, M. G. 1999, A&A, 341, L79
Varnière, P., Blackman, E. G., Frank, A., & Quillen, A. C. 2006, ApJ, 640, 1110
Zubko, V. G., Mennella, V., Colangeli, L., & Bussoletti, E. 1996, MNRAS, 282, 1321